Mechanistic events underlying odorant binding protein chemoreception

ARTICLE *in* PROTEINS STRUCTURE FUNCTION AND BIOINFORMATICS · MAY 2007

Impact Factor: 2.63 · DOI: 10.1002/prot.21307 · Source: PubMed

4 AUTHORS, INCLUDING:

Jérôme Golebiowski
University of Nice-Sophia Antipolis
50 PUBLICATIONS **341** CITATIONS
SEE PROFILE

Serge Antonczak
University of Nice-Sophia Antipolis
44 PUBLICATIONS **750** CITATIONS
SEE PROFILE

Sebastien Fiorucci
University of Nice-Sophia Antipolis
28 PUBLICATIONS **279** CITATIONS
SEE PROFILE

PROTEINS: Structure, Function, and Bioinformatics 67:448–458 (2007)

Mechanistic Events Underlying Odorant Binding Protein Chemoreception

Jérôme Golebiowski,* Serge Antonczak, Sébastien Fiorucci, and Daniel Cabrol-Bass
Laboratoire de Chimie des Molecules Bioactives et des Aromes, Faculté des sciences de Nice–Sophia Antipolis, Centre National de la Recherche Scientifique, UMR 6001, Université de Nice-Sophia-Antipolis, Parc Valrose, 28, avenue Valrose 06108 Nice Cedex 2, France

ABSTRACT **Odorant binding proteins (OBP's) are small hydrophilic proteins, belonging to the lipocalin family dedicated to bind and transport small hydrophobic ligands. Despite many works, the mechanism of ligand binding, together with the functional role of these proteins remains a topic of debate and little is known at the atomic level. The present work reports a computational study of odorants capture and release by an OBP, using both constrained and unconstrained simulations, giving a glimpse on the molecular mechanism of chemoreception. The residues at the origin of the regulation of the protein door opening are identified and a tyrosine amino-acid together with other nearby residues appear to play a crucial role in allowing this event to occur. The simulations reveal that this tyrosine and the protein's L5 loop are implicated in the ligand contact with the protein and act as an anchoring point for the ligand. The protein structural features required for the ligand entry are highly conserved among many transport proteins, suggesting that this mechanism could somewhat be extended to some members of the larger family of lipocalin. Proteins 2007;67:448–458.** © 2007 Wiley-Liss, Inc.

Key words: molecular dynamics; lipocalin; mechanism; odorant; simulation

INTRODUCTION

The proteins belonging to the superfamily of lipocalin are regarded as a paradigm for molecular recognition. Binding of ligands to members of the lipocalin protein superfamily is now quite well characterized. Although many of them show a clear ligand specificity, others, such as human Tear lipocalin, bovine β-Lactoglobulin, and odorant binding proteins (OBP's), demonstrate promiscuity.[1,2] More specifically, OBP's are considered as nonspecific binders. They are thought to participate in the olfaction process by carrying hydrophobic odorant molecules to the olfactory receptor, to trigger the sense of smell. Also, they are considered to be potentially involved in many other processes, such as pre-filters of odorants prior receptor binding[3–5] or even as detoxifiers to prevent receptor desensitization.[6] At the molecular level, OBP's share the common lipocalins structural motifs: a β-barrel structure, made up of eight strands (noted A to H), linked together by seven loops (L1 to L7), and connected to an α-helix. The β-barrel encloses an internal binding site, dedicated to small hydrophobic ligands, such as odorants or pheromones. It is considered that most of lipocalins bind their ligand targets through the opening of the cavity by a shift of the L1 loop. This leads to the denomination "open end" for this side of the lipocalins structures.[1,2]

Porcine OBP can be considered as typical of the OBP family and shows some well conserved amino acids with other OBP of the same class, notably with human OBP, as shown in Figure 1. Experimental structures of porcine OBP with different odorants have been solved by X-ray crystallography[7] and have already been the subject of a molecular dynamics (MD) study by us, considering 2,6-dimethyloct-7-en-2-ol or dihydromyrcenol (DHM) and 2-isobutyl-3-methoxy-pyrazine (IBMP) as ligands as shown in Scheme 1.[8] We have shown that, although the cavity is shielded from the solvent, openings have been observed, triggered by shifts of residues considered to constitute the door of the cavity, especially tyrosine 82. The knowledge of the OBP door location will be useful for further studies dealing with the potential interactions between OBP and the olfactory receptors.

Few works have supposed the existence of the OBP door, on the basis of static structures. Indeed, in the crystal structures of Aphrodisin and bovine OBP, existence of this door has been discussed on the basis of residue water-accessible surface considerations.[9,10] In the course of our article revision, restrained simulations without explicit solvent on the rat OBP with thymol as a ligand have been published.[11] The authors reported a transient opening of the OBP between strands D and E of the β-barrel throughout the ligand unbinding process.

The capacity to give a rationale to the role played by some protein residues will streamline the interpretation of the interactions underlying molecular biology. In a effort to unravel the biophysical aspects originating

*Correspondence to: Jérôme Golebiowski, PhD, Laboratoire de Chimie des Molecules Bioactives et des Aromes, Faculté des sciences de Nice-Sophia Antipolis, Centre National de la Recherche Scientifique, UMR 6001, Université de Nice-Sophia-Antipolis, Parc Valrose, 28, avenue Valrose, 06108 Nice Cedex 2, France.
E-mail: jerome.golebiowski@unice.fr

Received 10 July 2006; Revised 12 October 2006; Accepted 16 October 2006

Published online 6 February 2007 in Wiley InterScience (www.interscience.wiley.com). DOI: 10.1002/prot.21307

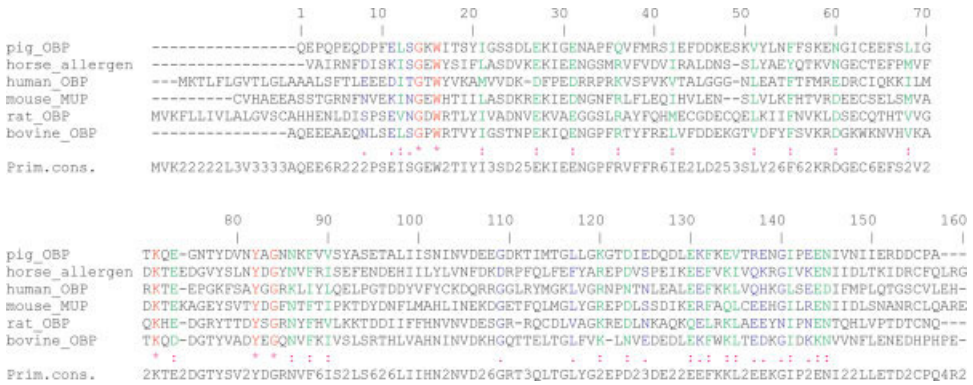

Fig. 1. Sequence alignment of porcine OBP with mammalian OBPs. Totally conserved residues are shown in red and strongly similar in green. The tyrosine residue (N° 82 in porcine OBP) is conserved among all the structures, from both the sequence and the structural point of view. [Color figure can be viewed in the online issue, which is available at www.interscience.wiley.com.]

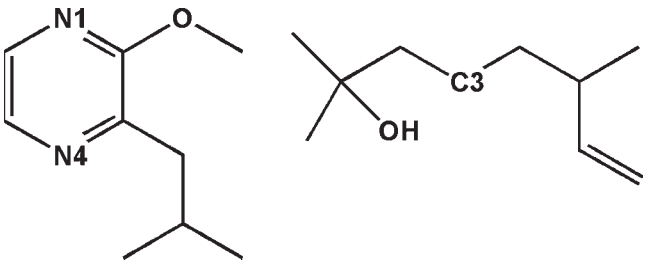

Scheme 1. IBMP and DHM chemical formulas.

OBP-ligand association as well as to describe the individual role played by several residues, well conserved among many sequences, we report the dynamic behavior of these systems throughout the ligand binding and unbinding processes.

METHODS

The MD simulations have been started considering X-ray structure taken from the PDB database (PDB id: 1E00 and 1DZK)[7] and were carried out using the AMBER 8.0[12] program in the isotherm isobar thermodynamic ensemble at 300 K. OBP/odorant complexes were neutralized by addition of 16 Na^+ counter ions, located in the most negative region of space, using the LEAP module of AMBER 8.0. The system was embedded in a periodic box containing 7823 and 7684 TIP3P water molecules for DHM and IBMP, respectively. The water phase was extended to a distance of 15 Å from any solute atom, leading to boxes whose dimensions were 71 × 64 × 72 $Å^3$ and 70 × 62 × 76 $Å^3$ for the DHM and IBMP complexes, respectively.

Simulations were carried out with the PMEMD module using SHAKE algorithm on bonds involving hydrogen atoms. A time step of 2 fs was applied. A 8 Å cut-off was applied to nonbonded van der Waals interactions, and the nonbonded pair list was updated every 15 steps. After having added the ions and the water molecules to the minimized complexes, 1000 steps of conjugate-gradient minimization keeping the complexes and the ions fixed were performed using particle mesh ewald (PME) summation. PME parameters are chosen to obtain a grid spacing close to 1 Å and a 9 Å direct space cut-off. The pressure and temperature coupling constants were fixed to 0.4 and 1 ps, respectively. The equilibration runs continued by an equilibration of 50 ps of PME dynamics keeping the solute fixed. Then, 1000 steps of minimization and 10 ps of MD simulation using a restraint of 20 kcal/(mol $Å^2$) on the solute atoms were performed, followed by four rounds of 1000 steps minimization reducing the restraints by 5 kcal/(mol $Å^2$) at each round, with 10 ps MD simulation. Further, the system was slowly heated from 100 to 300 K over a period of 15 ps. The equilibration was continued over 100 ps after these 15 ps.

Unless specified, the rms deviation (rmsd) was computed on the heavy atoms of the protein, to provide information on the structural integrity of the system upon ligand binding or unbinding. Additionally, the atomic fluctuation (also called the rms fluctuation) was computed to get insights into the mobility of a given residue throughout the simulation. The square of this value is proportional to the temperature B-factor and is notably valuable to identify the residues constituting the door of the protein, since their rmsf can raise large values upon binding or unbinding.

Unbinding Trajectories

To sample the unbinding of odorant from the protein, the use of biased simulations was necessary. Constrained simulations, where the microscopic system of interest is simulated in the presence of an artificial biasing window potential $w(\zeta)$, whose role is to enhance the sampling in the neighborhood of a given coordinate ζ have been performed. The biasing potential is used to keep the system around a confined region of coordinate ζ, to achieve a

more rigorous sampling of this region. Here, we use a harmonic potential of the form $w_i(\zeta) = k\ (\zeta - \zeta_i)^2$ centered on successive windows with a given value of ζ. The length and the size of each window were adjusted so that the system was allowed to relax sufficiently prior to another window. The different windows of the simulation were separated by a distance difference of 0.5 and 0.4 Å in the case of DHM and IBMP complexes, respectively. A value of force constant of 8 kcal/(mol · Å^2) was used. Examination of the impact of the simulation length in each windows, as well as the value of the force constant has been performed. Only minor differences are reported on the system behavior when the force constant used was 4 instead of 8 kcal/(mol Å^2). Concerning the length of each window, tests have also been made on the IBMP/OBP system. Here again, similar behaviors (trajectory, rms deviation) have been sampled between windows lasting 40 ps separated by 0.5 Å and windows lasting 360 ps separated by 0.4 Å. The latter simulation protocol involved a distance-restraint between the N1 atom of IBMP and the CA atom of Gly116, that was increased from 12.5 to 21.7 Å It led to a simulation time of 8.6 ns and was used for further structural analysis. The simulation for the unbinding of DHM was performed with a force constant of 8 kcal/(mol Å^2) between C3 atom of DHM and CA atom of Gly116. The simulation was made up of windows lasting 40 ps separated by a distance increment of 0.5 Å and led to a total simulation time of 2.4 ns, considered for further analysis.

Alternative Unbinding Trajectories

Other restrained-distances simulations have evaluated the influence of the choice of the restrained coordinate. Simulations trying to sample the unbinding of IBMP and DHM along alternative pathways excluding the role of Tyr82 were unsuccessful. These alternative pathways considered that the door could be made up of either L1-Loop or by residues belonging to the bottom (closed-end) of the protein calix. Because of too large denaturation of the protein structure throughout the unbinding processes, the simulations with either DHM or IBMP were stopped prior to the end of the process, after ~2 ns of simulation. These various simulations used a force constant of 8 kcal/(mol · Å^2), and sampled the unbinding process in windows of 40 ps separated by 0.5 Å. They are described in the following.

In a first attempt, a distance-restraint simulation forcing a distance elongation between the C3 atom of DHM and the CA atom of Pro34 was considered to try to sample the unbinding through the bottom of the calix. In a second simulation, we tried to use a distance restraint between the C3 atom of DHM and the centre of mass of residues Leu68, Phe88, Gly116, and Leu118, which represent the bottom of the binding cavity. In this simulation, we tried to sample the unbinding process via an transient opening of residues belonging to the L1 loop. In these two cases, a visual inspection of the protein structure leads us to give up these approaches. Indeed, the heavy atoms rmsd of the protein raised up to more than 5 Å, suggesting that the structure was clearly distorted upon the unbinding process. These simulations will not be described further. The only successful simulations involved Tyr82 and nearby residues as the protein door and seems similar to those observed very recently on a similar system.[11]

Binding Trajectories

The simulation runs to sample the binding of DHM into the protein cavity have been performed within two steps. First, a 1.2 ns restrained MD was performed to bring the odorant, initially in the bulk, close to the OBP (~5 Å from the closest residue) by applying a distance-restraint between DHM C3 atom and Gly116 CA atom with a force constant of 8 kcal/(mol · Å^2). This distance was initially of 32 Å. The total distance-restrained simulation consisted in 10 windows lasting 40 ps, where the distance was decreased by 0.5 Å at each step, to reach a final distance of 23 Å. Up to this point, a 8.3 ns equilibrium MD has been conducted, to let the system free to sample the energy surface without constraint. The total DHM-binding simulation time was thus 9.5 ns.

RESULTS AND DISCUSSION

Ligand Unbinding

The OBP cavity has already been described in previous studies, based-on X-ray structures.[7] The cavity is mainly composed of hydrophobic residues and totally occluded from water molecules. The various experimental structures showed that the odorants, depending on their chemical nature do not interact systematically with the same residues within the cavity. Nonetheless, some of them located in very different places around the cavity can be considered as crucial in the protein-ligand contact, such as Asn102, Phe88, and Ile21. The nonsystematic interactions lead the authors to conclude an opportunistic mode of binding. However, this viewpoint could be partly reconsidered, since a lysine residue, in a position equivalent to Asn102 has recently been shown to be crucial for the selectivity of a human OBP towards aldehydes,[13] suggesting that this region within the OBP cavities can play a more specific role than previously thought.

Here, the dynamic analysis leads to consider that Tyr82, in addition to its contribution to the protein cavity surface could also play a role in the regulation of the cavity door. This residue is located at the end of the OBP E-strand, just before the L5 Loop (see Refs. 1 and 2 for a detailed structural description of the protein). A hydrogen bond is present between the side-chain of this residue and the backbone of Pro34, belonging to the L1 Loop. This interaction contributes to close the upper bound of the protein calix and is found in every structures of both porcine and bovine OBP's complexed to various odorants.[7,10]

To examine the evolution of the β-barrel and the loops upon OBP–odorant interaction, simulations of odorant release from the protein cavity have been performed. The unbinding of the odorants from the OBP pocket cannot be sampled through classical MD simulation, since the binding free energy is negative (e.g. −38.5 kJ/mol, obtained experimentally for IBMP[14]) and the odorant is thus likely to remain within the cavity. Then, to explore such a mechanism, we use distance-restrained biased simulations, where the microscopic system of interest is simulated in the presence of an artificial biasing window potential whose role is to enhance the sampling in the neighborhood of a given structure along a reaction path. Here, the ligand is slowly pushed out of the cavity and the solvation feature of the ligand together with the structural deformation of the proteins is analyzed. During each window, keeping the odorant-OBP distance around a given value ζ, the system is able to relax on a sphere of radius ζ, thus sampling the lowest accessible free energy surface regions. These distance-restrained simulations have been carried out on the DHM/OBP and the IBMP/OBP complexes. The procedure is quite similar to the one performed on a similar system,[11] except that our simulations include explicit solvation. Our model, including explicit solvation, allows a better understanding of the role of solvent water in the neighborhood of the ligand throughout the binding and unbinding processes.

In the starting structures, the ligands are buried inside the hydrophobic protein cavity. This cavity is shielded from the aqueous bulk, notably by Tyr82 and Phe66, preventing water from entering the pocket.

For the unbinding of DHM, we have chosen to raise the distance between DHM and Gly116, (initially of 9.3 Å) since the latter is located at the bottom of the binding pocket. Various structure along the simulations are shown in Figure 2, as well as Tyr82-Pro34 distance, that can be used as a clue to define the end of the unbinding process. For DHM-Gly116 distances smaller than 14 Å, the odorant is considered to be inside the cavity and the protein structure deformation is deemed rather minor. However, a first event happens for a DHM-Gly116 distance of ∼14 Å, consisting in the breaking of Pro34-Tyr82 H—bond. This event allows water molecules to interact with the ligand and triggers the first contact of the hydroxyl group of DHM with bulk water molecules. The water molecules entered the cavity through a passage between residues 82–83 on one hand and Phe66 on the other. During this event, DHM shows a distance typical of a H-bond with Tyr82 backbone. Then, the ligand starts to shift Tyr82, Ala83, and Phe66 residues inside the bulk, and their atomic fluctuations can reach 2.9 Å, although they are computed to ∼1 Å in a classical equilibrium MD with the buried ligand. Pro34 remains quite faithful to its initial position. The ligand then slowly crosses through stands D and E of the β-barrel, slowly distorting the L5 loop and the E strand to reach out of the cavity. The number of coordinated water molecules to the ligand (data not shown) shows a first stage between 15 and 20 when the ligand is located between the residues constituting the door of the protein and then regularly increases to reach ∼20–25 for DHM-Gly116 distances larger than 22 Å. The ligand then continues its unbinding process, by going back and forth around strands D and E of the β-barrel and L5 loop. It is totally dissociated from the protein after ∼1.6 ns of simulation, that is, a distance of ∼21–22 Å between DHM and Gly116. The closest distance between DHM and the protein (Phe66 side-chain) oscillates around 7 Å.

Concerning the unbinding of IBMP, the same trend as for DHM is observed. The putative entry for the ligand into the cavity is also considered to be made up of residues ∼82–84. The trajectory reveals that when the odorant is slowly pushed out of the OBP cavity, Tyr82 and nearby residues show a regular structural drift. The H-bond between Pro34 and Tyr82 is also rapidly broken to let IBMP crossing between them, also drifting Ala83 from its initial position. The solvation of IBMP by the bulk water is definitely achieved after ∼1.5 ns of MD simulation, corresponding to a distance between IBMP N1 and Gly116 CA atom of 25 Å. The size of the ligand (IBMP is larger than DHM) does not appear to affect the extent of the deformation of the OBP structure, since the atomic fluctuation of Tyr82 is even lower in that case (rmsf of 2 vs. 2.9 Å for DHM). After the unbinding of the odorants, the OBP structure closely relates to the free OBP structure, recovering a Tyr82-Pro34 distance typical of a H-bond (Fig. 2). This connection contributes to shield the cavity from the solvent, where no water molecule is found.

At the end of the simulation, the protein structures are fitted to the free OBP structure obtained by X-Ray diffraction (PDB id: 1A3Y). These comparisons indicate a good recovery of the protein folding after the unbinding event. Indeed, the protein heavy atoms RMS deviation reaches 2.872 and 2.308 Å for DHM and IBMP unbound complexes, respectively.

These restrained MD simulations revealed that the interaction between porcine OBP and its ligand occurs through the shift of residues mainly located at the junction between the strands D and E and the L1 and L5 loop. Tyr82 appears to be especially involved in the unbinding process and can be considered as the gate of the OBPs, because of its large conservation among this family.

Ligand Binding

To assess the role of this part of the protein throughout the binding process, we have tried to sample the binding of DHM, in an equilibrium simulation, starting from the end of the simulation that initially brought the ligand close to the protein by means of an umbrella sampling simulation. The sampling of such a binding process, considered as a "reactive" path in a given system is very difficult to obtain, since the system can sample the energy surface for a long time prior to an interesting structural event sampling. However, when such an event can be observed, it can bring much information concern-

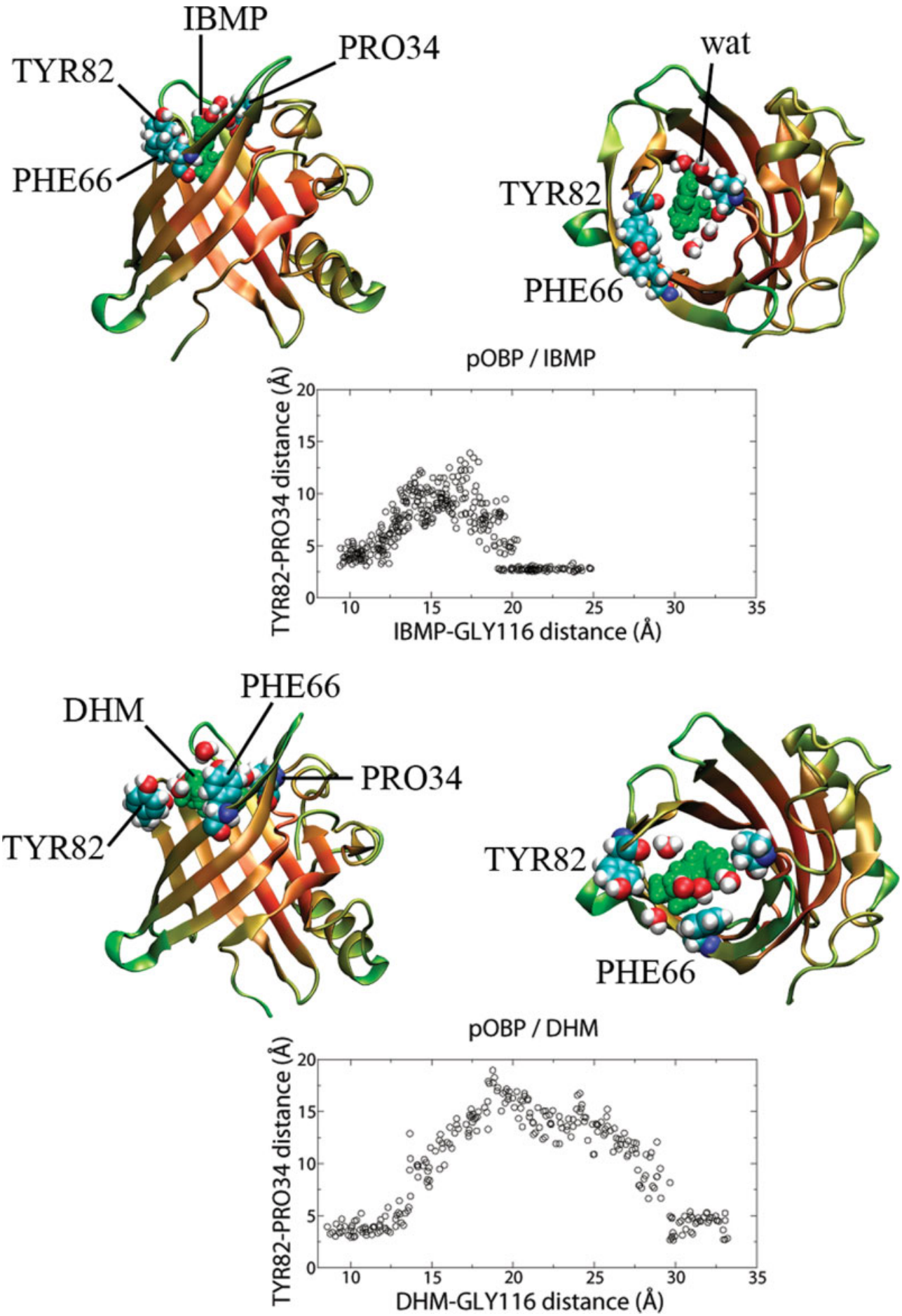
IBMP
PRO34
TYR82
PHE66
wat
TYR82
PHE66
pOBP / IBMP
TYR82-PRO34 distance (Å)
IBMP-GLY116 distance (Å)
PHE66
DHM
PRO34
TYR82
TYR82
PHE66
pOBP / DHM
TYR82-PRO34 distance (Å)
DHM-GLY116 distance (Å)

Figure 2.

ing the "real" dynamic behavior of the system since no bias is included in the simulation protocol. In our case, the binding simulation was successful and is reported in the following.

The odorant is initially positioned at 33 Å from the bottom of the cavity (here considered to be Gly116 CA atom) in front of the strands D and E of the β-barrel structure of the protein. During the first phase of the simulation, lasting 1.2 ns, the ligand is artificially brought close to the protein, by applying a force between DHM and Gly116.

This restrained MD was stopped when the distance between DHM and the closest residue of the OBP was 5 Å. Up to this point the ligand is fully solvated and no drift of the protein structure neither of residues side-chains are observed, suggesting that the odorant is far enough away from the protein to consider this structure as a valid starting point for further equilibrium simulations. The binding cavity is fully shielded from the solvent, and unbiased simulations have been carried out to sample the ligand association by the protein. This process has been observed in two distinct simulations. The resulting final structures are both similar and very close to the experimental one, with protein heavy atom RMS deviation with respect to the experimental X-ray structure computed to less than 2.0 Å in each case. For simplicity purposes, only one simulation will be described in the following.

The number of first coordination shell water molecules is used as a clue for defining the end of the binding process. This feature, together with the distance between the odorant and the OBP cavity bottom are reported in Figure 3 and simulation snapshots are gathered in Figure 4.

At the beginning of the equilibrium simulation, DHM is located at 8.6 Å from Tyr82 hydroxyl group, near the L5 and L1 loops. The distance between DHM C2 atom and CA atom of Ala83, a residue considered as representative of the L5 loop is 5.00 Å, and the distance between the hydroxyl oxygen atom of DHM and the backbone of Pro34 (the closest residue belonging to the L1 loop) is 4.98 Å. The distance between both CG atoms of Tyr82 and Phe66 oscillates around 8.5 Å and samples distances of ~6.5 Å, typical of the X-ray structures values (6.16 and 6.31 Å in the free OBP (PDB id: 1A3Y) and DHM/OBP complex (PDB id: 1E00), respectively).

During 200 ps, the odorant goes back and forth around this region (near the OBP door) and starts to interact with residues lining the surface of the OBP. After this period, the previously defined distance reaches

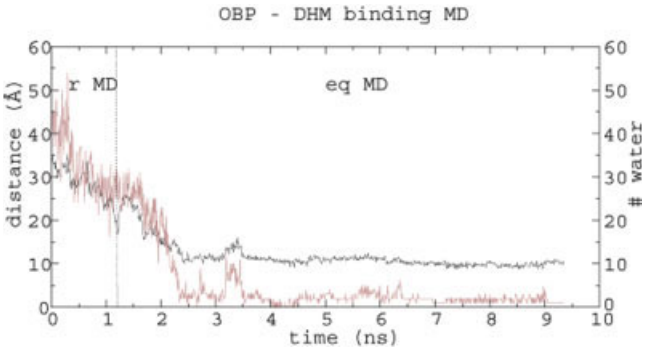

Fig. 3. Distance (in Å, black coloured) between the CA atom of Gly 116 and the Oxygen atom of DHM throughout the binding process, and number of water molecules in a sphere of radius 3.5 Å around the solute (brown coloured). Periods corresponding to the restrained MD (r MD) and equilibrium MD (eq MD) are indicated. [Color figure can be viewed in the online issue, which is available at www.interscience.wiley.com.]

5.9, 6.0, and 16.2 Å between DHM and Tyr82, Ala83, and Pro34, respectively. At this point, no water molecules are located within the OBP cavity that is still shielded from the bulk, mainly by Tyr82 and Phe66 side-chains. The distance between Tyr82 and Pro34 oscillates around 6 Å, with only few interactions, revealing a weakly altered structure. DHM all-atom rmsd evolution with respect to the X-ray DHM is shown in Figure 5. Its represents not only variation in ligand conformation but also difference in ligand position and orientation with respect to the protein. The starting values are high at the beginning of the simulation, since the odorant is far away from its final position within the binding cavity. Then, the rmsd rapidly decreases to reach values close to 2.5 Å, indicating that the final orientation and position of the ligand is quite similar to that found in the X-ray structure.

The odorant starts to enter the cavity through a shift of the residues belonging to the strands D and E and the L5 loop, particularly Tyr82 and Ala83, whose heavy-atoms atomic fluctuations both reach 2.5 Å. During this time, only few interactions with residues belonging to the L1 loop can be observed and Tyr82-Pro34 distance samples values larger than 10 Å. At this point, the ligand is positioned vertically above the β-barrel, with the hydrophobic part towards the L1 loop of the lipocalin, creating a weak H-bond with Pro34 backbone oxygen atom that was previously interacting with Tyr82. The all atoms rmsd for the DHM is computed to ~17 Å at this point (Fig. 5). The odorant slowly gets inside the

Fig. 2. Snapshots for the unbinding simulations of IBMP and DHM from porcine OBP. Side and top view of the moment corresponding to the exit of the odorant from the cavity. The odorant are shown in green spheres. Tyr82, Phe66, and Pro34 are shown as balls, coloured by atom type (H: white, C: cyan, O: red, and N: deep blue), the remainder of the protein is shown as ribbon, coloured by position with respect to the protein surface (green: at the surface, red: buried within the cavity). Water molecules within 3 Å of any odorant atom are shown (4 in the case of IBMP and 6 in the case of DHM). For each system, the distance between Pro34 and Tyr82, which is typical of the cavity closure is shown as a function of the restrained distance (IBMP N1 atom–GLY116 CA atom and DHM C3 atom–GLY116 CA atom). [Color figure can be viewed in the online issue, which is available at www.interscience.wiley.com.].

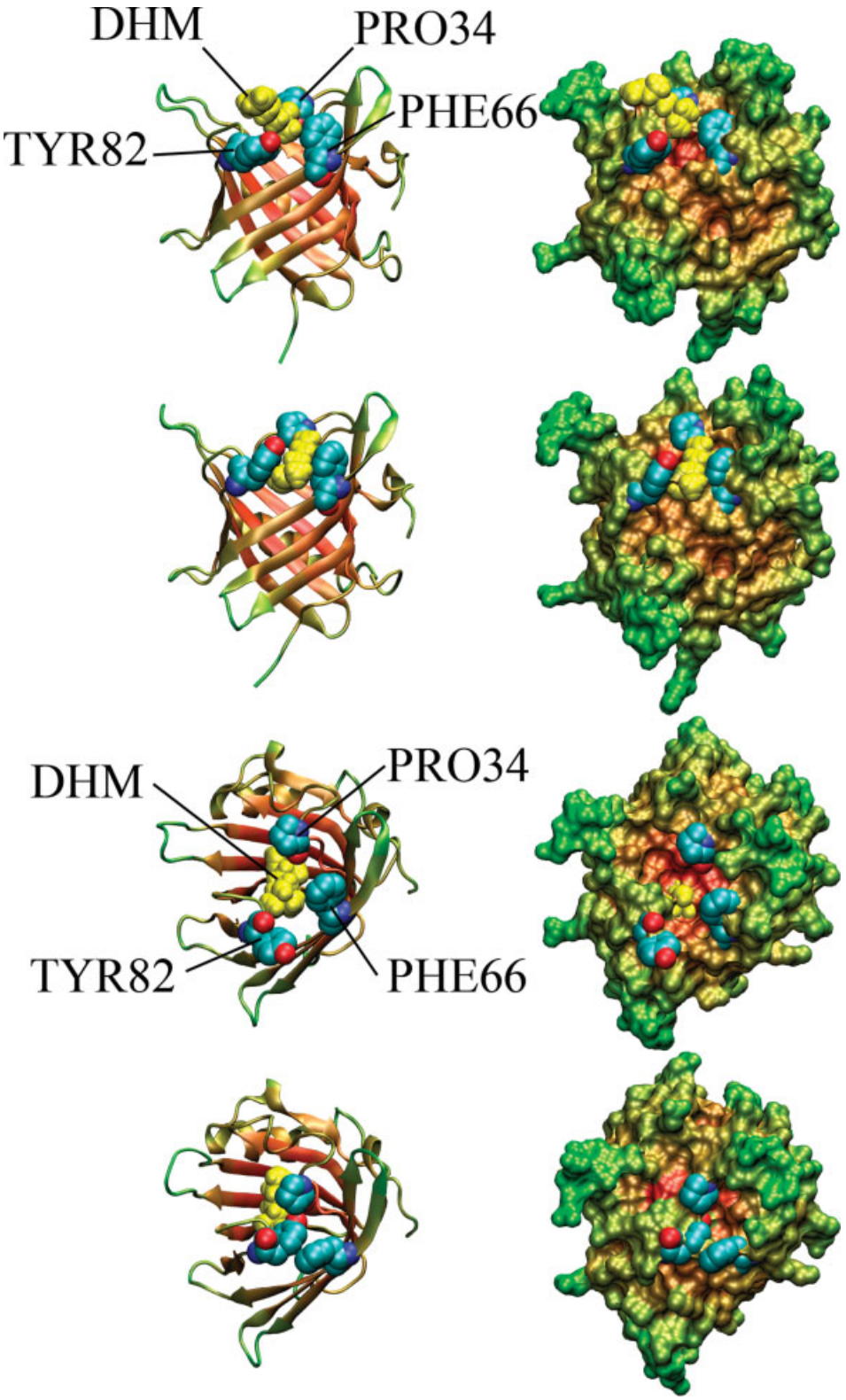

Fig. 4. OBP/DHM system at 1.2 ns and 2 ns (side views), 3 ns and 9.4 ns (top views). Tyr82 and Phe66, Pro34 as well as DHM are shown in balls. DHM is yellow colored. other residue are colored by position, with respect to the protein surface (green: at the surface, red: buried within the cavity) The snapshots shown on the right represent the residues volume, while the snapshots on the left represent the secondary structure with only Tyr82, Pro34, Phe66, and DHM in balls.

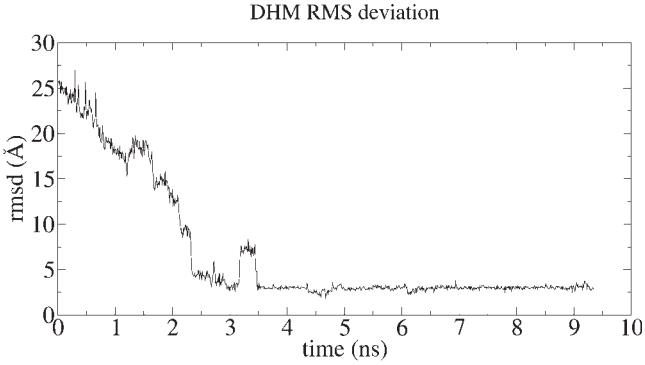

Fig. 5. All atoms rmsd (Å) between the X-ray and simulated DHM after superposition of the X-ray and simulated protein atoms throughout the binding trajectory.

cavity, losing its interactions with the bulk water molecules (Fig. 3). After a few hundred ps, the hydrophobic part of the odorant is close to the bottom of the cavity, here characterized by Phe87 and the structure closely relates to the X-ray structure, although Tyr82 and Phe66 still show some mobility. The all atom DHM RMS deviation rapidly decreases to reach values weaker than 5 Å. 2.3 ns after the first contact, DHM regularly samples a double H-bond network with Asn86 and Asn102, as previously seen in MD simulations.[8] The distance between the oxygen atom of DHM and the oxygen atom of the side chain of Asn102 lowers to 2.7 Å. For a short period going from 3.16 to 3.48 ns, DHM goes back and forth within the cavity and its RMS deviation with respect to the X-ray ligand increases to reach values up to 8.3 Å, as shown in Figure 5. 5 ns after the first contact, a final reorganization of Tyr82 (still in the bulk) towards Pro34 leads to a structure identical to the X-ray structure. The interaction between Tyr82 and Pro34 is then recovered, with the typical distance of 2.8 Å between the oxygen atoms of both the tyrosine side-chain and the proline backbone. The DHM-Gly116 distance oscillates around 10 Å and the structure does not evolve until the end of the simulation. During the binding process, the distance between CG atoms of Tyr82 and Phe66 remains in the range 9.5–11.5 Å. For a short period, corresponding to the crossing of DHM between strands D and E of the OBP, this distance rises to 13.5 Å, then, this distance lowers to ~6 Å, as in the various X-ray structures with different buried ligands. The heavy-atoms RMS deviation between the structure at the last point of the simulation (corresponding to a time of 9.5 ns) and the experimental X-ray one (PDB id: 1E00) is 1.83 Å.

During the approach of the ligand towards the protein entry and the binding process, we have not detected any highly ordered water cluster in the neighborhood of the system. Such a solvation feature would have restricted the flexibility of the protein, and thus increased the conformational entropy upon binding as thought in a study of the mouse MUP OBP.[15] This is not the case here and water molecules show large mobility around the protein system and no special H-bonding can be observed with long residence time between the protein entry and bulk waters. On the contrary, at the beginning of the entry process, the odorant is accompanied by four to five water molecules also entering the cavity previously devoid of any water molecule. These molecules take a long time to be withdrawn from the hydrophobic cavity. The residence time for the last water molecule being in contact with the ligand is estimated to ~2 ns, suggesting that very long simulation time is needed to relax the system after the binding process. Note nonetheless that from an energetic point of view, the binding of ligand within OBP is not considered to be controlled by hydrophobic effects, since the interaction energy is enthalpy-driven.[16]

Although the entry of DHM within the cavity can be considered as achieved after ~2.5 or 3 ns, the solvation feature of DHM stabilizes after a simulation time of 6.5 ns, with only one or two water molecules remaining in contact with DHM after this period (Fig. 3). These solvent molecules can thus be considered as belonging to the binding site since they do not affect the structural features of the odorant–protein interaction and show long residence time. Nonetheless, these water molecules are not present in the X-ray structure, suggesting that they could be withdrawn if longer simulation would be performed or that they are not detected, because of a large mobility. Such a behavior has already been observed for the MUP-I protein, where two water molecules are present in the X-ray structure containing a thiazole derivative[17] although no water is found when the ligand is more bulky, such as IBMP.[16] The size of our ligands suggests that we are in the second case, as the MUP/IBMP complex. Nonetheless, the presence of these one or two water molecules does not call into question the binding process previously sampled.

A Model for Initiation of OBP Chemoreception

These joint biased and equilibrium MD simulations can be assembled into a detailed mechanistic model of mammalian OBP chemoreception. The results enlighten the molecular mechanisms underlying ligand uptake and release and emphasize the dynamic role played by Tyr82, Ala83, belonging to the L5 loop, Pro34, belonging to the L1 loop, and Phe66, belonging to strand D.

Tyrosine side-chain and the proline 34 backbone together act as anchor points to initiate the process of odorant/OBP association through hydrophilic interactions. This first event is coupled to additional structural events at the other side of the OBP door (notably a phenylalanine), as the odorant is slowly getting closer to the OBP door. Tyr82 and Phe66 slowly move from their initial position towards the bulk to let the place for the ligand to enter the binding pocket. Then, they recover their initial positions, and shift the odorant from the remaining water molecules still present in its neighborhood. The ligand is then buried inside the OBP hydrophobic cavity and the shifted residues recover their ini-

tial positions. Minor structural drifts caused during the binding and unbinding processes are reported, the structure rapidly recovering its typical β-barrel fold, occluding the cavity from the solvent.

OBP's can be found as a monomer or a dimer depending on experimental conditions. At physiological pH, porcine OBP is a dimer, but is found as a monomer when the pH drops.[14] The question of the necessity of the OBP to be in a dimeric form for proper function can be considered. Indeed, the bovine OBP presents a so-called domain swapping, connecting two OBP sub-units of a dimer, that can thus not be disconnected, contrarily to those of other mammalians.[18,19] However, experimental results have shown that only a single odorant binds to the dimer in solvent. In the dimeric X-ray structure, Tyr82 in one of the sub-units is shifted from the bulk by the α-helix of the second sub-unit. Such a structural organization could explain that, if the protein is found as a dimer, one of the sub-units is unable to bind a ligand by the shift of Tyr82, resulting in a single odorant per dimer as it is the case in many studies.[14,21] Here, the binding process has been sampled without any constraint on an OBP monomer, suggesting that the odorant binding process does not absolutely require the OBP to be in a dimeric form and that this dimerisation is only due to strong electrostatic interactions between the two sub-units.

The presence of the tyrosine residue, located between strands D and E of the barrel appears to be crucial for the binding of the ligand. The structural drift of the L1 loop is deemed rather minor, but one of its residue backbone oxygen atom (Pro34) undergoes a H-bond interaction with the odorant in the early steps of the binding process. This residue interacts with the tyrosine gate hydroxyl group, to keep the structural integrity of the OBP and to prevent water from entering the binding pocket. Note that Pro34 conservation amongst various OBP's is not absolutely required, since only its backbone atoms are involved in the interaction.

Concerning tyrosine, it is able to drive hydrophobic effects through its aromatic ring, and also hydrophilic interaction via its hydroxyl group. It appears to be particularly well suited to play the role of a door in such proteins. Both of these interactions contribute to occlude the binding site from the bulk, hampering hydration of the internal cavity. This residue is strictly conserved among several sequence alignments, including human OBP, suggesting a systematic binding of the target through a tyrosine-type gatekeeper residue. When this residue is not conserved in some members of the OBP family, it is often replaced by a phenylalanine residue and one can thus suppose that the protein entry door is conserved at least from a structural point of view.[9]

The quantification of entropic terms arising from ligand-protein association remains a intense subject of investigation and MD simulations, as well as NMR studies appear to be particularly well suited for such a kind of analysis. Although this study is not directly performed for such considerations, since it would have required additional and dedicated approaches, such as quasi-harmonic or normal-mode calculations, one can nonetheless bring some general qualitative insights, based on the characteristics of our system.

The major term favoring association between a protein and a hydrophobic ligand is described to be the hydrophobic effect. The weak affinity between the water molecules and the ligand are thought to result in a spontaneous ligand exclusion from the bulk. When the ligand is close enough from the protein, opportunistic interactions finally bring the ligand close to residues constituting the door of the protein. Note nonetheless that, totally counter intuitively, the solvation features of the ligand does not appear to be crucial in the binding energetics, since the whole binding process was shown to be not entropy-driven on a closely related OBP/odorant system.[20] Indeed, the favorable entropic contribution of ligand desolvation was shown to be insufficiently important to overcome the largely unfavorable entropy arising from ligand loss of degrees of freedom.[22] Such an effect can be compensated by protein solvation features, notably by the release of ordered water molecules within or at the entrance of the binding pocket. This effect favors association since it increases the dynamics of side-chains distal to the binding site. Although the term arising from protein dynamics is constant for a given protein, the ligand loss of degree of freedom naturally depends on the number of rotors of the bonded ligand (the larger the number of rotors, the higher the entropy penalty upon binding). Such considerations agree with a previous work, reporting that the length and the size appears as a crucial structural criterion for OBP/odorant recognition.[21,23] On a MUP-1/IBMP study, the overall unfavorable entropic contribution of binding was reported to be close to ~10 kJ/mol. This quite low value is explained as the result of a strongly unfavorable contribution arising from the loss of degree of freedom of both the ligand and the protein and another favorable contribution brought by the release of ordered water molecules initially present within the binding pocket. One can consider that our system should show a similar energetic value. Nonetheless, the release of ordered water molecules has not been clearly evidenced in our simulation.

OBP's share commons structural characteristics with their superfamily, the lipocalins. The presently described ligand binding mechanism involves residues and/or structures whose equivalent can be found among all the lipocalins. The β-strands, and more particularly the shape of the junction between the D and E strands is a constant structural motif. Note also that a joint NMR and MD work on β-Lactoglobulin reported the involvement of L5 loop (also called EF loop) in the ligand binding process.[24] The structural drift originating this binding are due to the protonation of a glutamate residue and thus pH-dependent.

In the Bombyx mori, the ligand binding and release is also thought to be due to a pH-dependent conformation of the pheromone binding proteins (PBPs), a sub-family of OBPs.[25] It is believed that as the protein-ligand com-

plex reaches near the membrane, the pH drops and some of the proteins residues become protonated. This effect triggers a "coil-to-helix" conformational change of a given part of the protein, which contributes to the release of the odorant from the binding pocket towards the olfactory receptor. After that structural event, the PBP is released from the membrane and recover its initial conformation at higher pH, to be ready for an additional cycle of ligand transport.[26] In PBP's, the acidic residues (glutamate or aspartate) believed to be involved in this protonation/deprotonation process are conserved amongst many sequences. The question whether such a structural behavior can exist for mammalian OBP's remains unclear, since to date, no alternative structure to those determined by X-ray experiments has been reported for these proteins. Such glutamate and aspartate residues are also found to be well conserved amongst mammalians OBP's, and they interestingly belong to the L1 loop (residues Glu27 and Glu31 in Fig. 1). This work has just shown the influence of this Loop on ligand binding and release. With a pH drop at the membrane surface, the glutamate residues of this loop would become protonated, neutralizing their negative charge and increasing their hydrophobic character. They would thus be likely to perturb the local folding of the loop, also perturbing the tyrosine gate, making it easier for the ligand to be ejected from the binding pocket. To gain more information on the potential role of such residues in the binding and release at the membrane surface, additional insights could be obtained either by means of NMR or MD simulations in solution, where the pH can be controlled.

In a general manner, the knowledge of the OBP door location and function will be useful for further studies dealing with the interaction between OBP and the olfactory receptors. Although the binding of an OBP to a human OR has been characterized experimentally,[27] no clue has been given considering the molecular aspects underlying the binding process. Further, for ligand transfer between the OBP and an OR, the docking of both proteins will have to let the OBP door free for the ligand to cross from one to the other protein. This mechanistic event probably requires an allosteric effect to open the OBP door, since no spontaneous odorant unbinding has ever been observed. This effect could be due to either the receptor or to a pH-dependent conformation. Above all, Tyr82 as well as residues involved in the L1 and L5 loops are likely to play a crucial role in such a mechanism.

The determination of the dynamical behavior of such biomolecular systems might help in the understanding of their role and function. To this end, the results of theoretical simulations, like those carried out in this work, will be extremely useful.

ACKNOWLEDGMENTS

We thank the CINES and the CMIM for provision of computer time. JG thanks Dr. C. Nespoulous, Dr. S. Antoniotti, and the referees for helpful suggestions concerning the manuscript.

REFERENCES

1. Flower DR. The lipocalin protein family: structure and function. Biochem J 1996;318:1–14.
2. Flower DR. Multiple molecular recognition properties of the lipocalin protein family. J Mol Recognit 1995;8:185–195.
3. Löbel D, Strotmann J, Jacob M, Breer H. Identification of a third rat odorant-binding protein (OBP3). Chem Senses 2001;26:673–680.
4. Pevsner J, Reed RR, Feinstein PG. Snyder SH molecular cloning of odorant-binding protein: member of a ligand carrier family. Science 1988;241:336–339.
5. Löbel D, Marchese S, Krieger J, Pelosi P, Breer H. Subtypes of odorant-binding proteins—heterologous expression and ligand binding. Eur J Biochem 1998;254:318–324.
6. Boudjelal M, Sivaprasadarao A, Findlay JB. Membrane receptor for odour-binding proteins. Biochem J 1996;317:23–27.
7. Vincent F, Spinelli S, Ramoni R, Grolli S, Pelosi P, Cambillau C, Tegoni M. Complexes of porcine odorant binding protein with odorant molecules belonging to different chemical classes. J Mol Biol 2000;300:127–139.
8. Golebiowski J, Antonczak S, Cabrol-Bass D. Molecular dynamics studies of odorant binding protein free of ligand and complexed to pyrazine and octenol. J Mol Struct (Theochem) 2006;763:165–174.
9. Vincent F, Löbel D, Brown K, Spinelli S, Grote P, Breer H, Cambillau C, Tegoni M. Crystal structure of Aphrodisin, a sex pheromone from female hamster. J Mol Biol 2001;305:459–469.
10. Vincent F, Ramoni R, Spinelli S, Grolli S, Tegoni M, Cambillau C. Crystal structures of bovine odorant-binding protein in complex with odorant molecules. Eur J Biochem 2004;271:3832–3842.
11. Hajjar E, Perahia D, Débat H, Nespoulous C, Robert CH. Odorant binding and conformational dynamics in the odorant-binding protein. J Biol Chem 2006;281:29929–29937.
12. Case DA, Pearlman DA, Caldwell JW, Cheatham TE, III, Ross WS, Simmerling C, Darden T, Merz KMJ, Stanton RV, Chen A, Vincent JJ, Crowley M, Tsui V, Radmer R, Duan Y, Pitera J, Massova I, Seibel GL, Singh UC, Weiner P, Kollman PA. University of California, San Francisco, AMBER8.0.
13. Tcatchoff L, Nespoulous C, Pernollet JC, Briand LA. Single lysyl residue defines the binding specificity of a human odorant-binding protein for aldehydes. FEBS Lett 2006;580:2102–2108.
14. Burova TV, Choiset Y, Jankowski CK, Haertle T. Conformational stability and binding properties of porcine odorant binding protein. Biochemistry 1999;38:15043–15051.
15. Zidek L, Novotny MV, Stone M. Increased protein backbone conformational entropy upon hydrophobic ligand binding. Nat Struct Biol 1999;12:1118–1121.
16. Bingham RJ, Findlay JBC, Hsieh SY, Kalverda AP, Kjellberg A, Perazzollo C, Philipps SEV, Seshardi K, Trinh CH, Turnbull WB, Bodenhausen G, Homans SW. Thermodynamics of binding of 2-methoxy-3-isopropylpyrazine and 2-methoxy-3-isobutylpyrazine to the major urinary protein. J Am Chem Soc 2004;126:1675–1681.
17. Timm DE, Baker LJ, Mueller H, Zidek L, Novotny MV. Structural basis of pheromone binding to mouse major urinary protein (MUP-I). Protein Sci 2001;10:997–1004.
18. Bianchet MA, Bains G, Pelosi P, Pevsner J, Snyder SH, Monaco HL, Amzel LM. The three-dimensional structure of bovine odorant binding protein and its mechanism of odor recognition. Nat Struct Biol 1996;3:902–906.
19. Tegoni M, Ramoni R, Bignetti E, Spinelli S, Cambillau C. Domain swapping creates a third putative combining site in bovine odorant binding protein dimer. Nat Struct Biol 1996;3:863–867.
20. Barrat E, Bingham RJ, Warner DJ, Laughton CA, Philipps SEV, Homans SW. van der Waals interactions dominate ligand-protein association in a protein binding site occluded from solvent water. J Am Chem Soc 2005;127:11827–11834.

21. Pevsner J, Hou V, Snowman AM, Snyder SH. Odorant-binding protein, characterization of ligand binding. J Biol Chem 1990;265: 6118–6125.
22. Shimokhina N, Bronowska A, Homans SW. Contribution of ligand desolvation to binding thermodynamics in a ligand-protein interaction. Angew Chem Int Ed Engl 2006;45:6374–6376.
23. Nespoulous C, Briand L, Delage MM, Tran V, Pernollet JC. Odorant binding and conformational changes of a rat olfactory-binding protein. Chem Senses 2004;29:189–198.
24. Ragona L, Fogolari F, Catalano M, Ugolini R, Zetta L, Molinari HEF. Loop conformational change triggers ligand binding in β-lactoglobulins. J Biol Chem 2003;278:38840–38846.
25. Horst R, Damberger F, Luginbuhl P, Guntert P, Peng G, Nikonova L, Leal WS, Wuthrich, K. NMR structure reveals intramolecular regulation mechanism for pheromone binding and release. Proc Natl Acad Sci USA 2001;98:14374–14379.
26. Lautenschalger C, Leal WS, Clardy J. Coil-to-helix transition and ligand release of *Bombyx mori* pheromone-binding protein. Biochem Biophys Res Commun 2005;335:1044–1050.
27. Matarazzo V, Zsürger N, Guillemot JC, Clot-Faybesse O, Botto JM, Dal Farra C, Crowe M, Demaille J, Vincent JP, Mazella J, Ronin C. Porcine odorant-binding protein selectively binds to a human olfactory receptor. Chem Senses 2002;27: 691–701.